

# Effects of bottom quark induced processes on polarized $W^+W^-$ production at the LHC at NLO

Duc Ninh Le, Thi Nhung Dao

Faculty of Fundamental Sciences, PHENIKAA University, Hanoi 12116, Vietnam

E-mail: ninh.leduc@phenikaa-uni.edu.vn

**Abstract.** In this report we discuss the definition of the polarized cross sections of the inclusive  $W^+W^-$  production at the LHC. Results at the level of next-to-leading order (NLO) QCD+EW accuracy, published in our recent paper, are presented to highlight the effects of bottom-quark induced processes. Compared to the unpolarized case, the bottom-induced effects after the subtraction of the on-shell top-quark contribution are more sizable for the doubly-longitudinal polarization.

## 1. Introduction

Proton-proton collisions at the LHC provide us valuable information into the world of fundamental particles. A lot of data have been collected and stored, and more are being produced with the current LHC run-3, which is scheduled until June 2026. The current colliding energy of the LHC is 13.6 TeV, increased from the 13 TeV value of run-2. These data can be used to explore the limits of the Standard Model (SM), which is based on the local gauge symmetry of  $SU(3)_C \otimes SU(2)_L \otimes U(1)_Y$  and the electroweak spontaneous symmetry breaking mechanism.

Among many different kinds of measurements, polarization measurements of massive gauge boson pair production at the LHC have recently attracted a significant amount of attention. ATLAS and CMS have published results of polarized diboson production in [1, 2] ( $WZ$ ) and [3] ( $ZZ$ ), and [4] (same-sign  $WWjj$ ). These efforts help us to explore unknown regions of particle physics, including: (i) the on-shell and off-shell boundary, (ii) different polarization modes and their interference.

Differently from the unpolarized case, polarization measurements must somehow separate the polarized cross sections from the unpolarized cross section. As the detectors can only provide information of the decay products, an additional step must be done to define polarizations in the measurement. This definition must give a concrete result for kinematic distributions of the decay products. This set of polarized distributions (named polarization templates), which can only be produced by simulation (e.g. using the SM), is the definition of the polarizations. If all unpolarized differential cross section measurements can be fitted by a sum of those polarization templates (including a template for their interference), then we say that the polarization model is correct and the polarization fractions ( $\sigma_{\text{pol-i}}/\sigma_{\text{unpol}}$ ) can be extracted from a fit to a chosen distribution (in principle, “any” kinematic distribution can be chosen, but some give better results than others due to different discrimination power, e.g. a boosted-decision-tree score distribution was chosen in [3]. This step can be done for the whole fiducial phase space or bin-wise.). In reality, off-shell effects are included in the unpolarized cross section measurements.

Therefore, these effects must be accounted for by using a separate template or including them in the background as done in [3].

It then becomes clear that polarization templates are one of the most important information in a polarization measurement. Ideally, these templates should be published together with the paper, or at least a description of them should be provided.

It is also clear that polarization templates depend on the theoretical model used in the simulation and the precision of the cross section calculation. The precision level of the simulation changes with time. This is of course true for any measurements (e.g. the background estimation using simulation changes with new updates), but the impact on polarization measurements may be greater than on the unpolarized cases.

As parton showers are expected to be different for different polarized  $VV$  modes, these effects have to be calculated separately for each polarization template. Work in this direction has been done, see [5, 6, 7]. Hadronization is also different for different polarizations, this effect is however expected to be much smaller than those of parton showers.

Kinematic cuts affect polarization states differently. To allow for future (re-)analyses with different lepton kinematic cuts, a good strategy is to generate events for different polarization states with an inclusive cut setup (e.g. including only  $m_{4l} > M_V + M_{V'}$  cut) and store these events. At the analysis level, analysis cuts are then applied to these inclusive polarized events to produce fiducial-level templates to be used in the final fit. The extracted polarization fractions depend on the analysis cuts as the cuts affect  $\sigma_{\text{pol-i}}$  and  $\sigma_{\text{unpol}}$  differently.

Since parton showers can only improve results in the soft and collinear regions, fixed order calculations are needed for a better description of the hard regions. Next-to-leading order (NLO) and beyond calculations of the polarized cross sections are therefore important. Progress has been made in this direction as well.

We mention here the recent development in the calculation of higher-order corrections to the polarized  $VV$  production cross sections with fully leptonic decays. The first NLO QCD corrections were done in [8] for the  $W^+W^-$  case. These results were soon extended to the  $ZZ$  case [9], including the NLO electroweak (EW) corrections this time. This  $ZZ$  work is important as it provides new on-shell mappings (see Section 2)  $1 \rightarrow 2$  and  $1 \rightarrow 3$ , which are crucial for the definition of the polarization templates. The  $1 \rightarrow 2$  mapping is used for the leading order (LO)  $V$  decays, while the  $1 \rightarrow 3$  mapping is for the NLO  $V$  decays occurring in the NLO EW corrections. Using these new on-shell mappings, the NLO EW corrections for the  $WZ$  case were completed in [10, 11]. This is a major improvement compared to the  $ZZ$  case because the  $WZ$  production involves an on-shell charged current where a photon can be radiated off the intermediate on-shell  $W$ . This radiation introduces soft divergences which must be canceled with the counter parts in the virtual corrections of the  $WZ$  production and  $W$  decay amplitudes. The  $WZ$  calculation was then straightforwardly extended to the  $W^+W^-$  case in [12, 13]. A further step was recently done for the same-sign  $W^+W^+jj$  production [14], where final-state photon radiation is more complicated than the inclusive  $W^+W^-$  case as interferences between jet-photon radiation amplitudes and lepton-photon radiation amplitudes occur. Treatment of these radiations requires modifications of the decay momenta. These modifications interplay with the on-shell mappings, therefore require careful attention. Moreover, the important next-to-next-to-leading order (NNLO) QCD corrections for the polarized  $W^+W^-$  production were calculated in [15]. The case of semi-leptonic decays has been considered in [16].

In this report, which is a contribution to the proceedings of the **PIAS workshop 2024: Physics at different scales** (Hanoi, Vietnam, 2024), we consider the case of inclusive  $W^+W^-$  production and focus on the definition of the polarized  $W^+W^-$  pair production. This is the signal part. The definition used in this work is in accordance with the common definition of the unpolarized  $W^+W^-$  pair production used in the literature and in the experimental measurements. This definition requires the subtraction of the top-quark contribution. This

subtraction has to be done for individual polarizations and has been recently achieved by us in [17] at NLO QCD+EW accuracy. The presentation presented here is based on this result. In addition, we take this opportunity to discuss in more detail the definition of the inclusive polarized  $W^+W^-$  production signal. This discussion is provided in Section 2. Important numerical results are then presented in Section 3. Finally, a short conclusion is provided in Section 4.

## 2. Method of calculation

The signal process is

$$p(k_1) + p(k_2) \rightarrow W^+(q_1)W^-(q_2) \rightarrow e^+(k_3) + \nu_e(k_4) + \mu^-(k_5) + \bar{\nu}_\mu(k_6), \quad (1)$$

where the final-state leptons are the decay product of the intermediate  $W^+W^-$  system. This is illustrated by a Feynman diagram in Fig. 1.

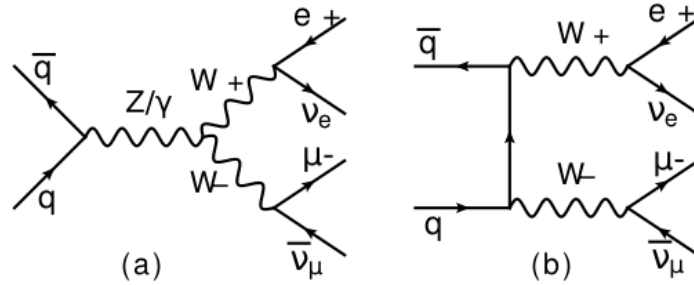


**Figure 1.** Tree-level Feynman diagrams describing a  $W^+W^-$  resonant signal process at the LHC.

A  $W$  boson can decay into leptons (33%) or quarks (67%). The hadronic final state has a higher rate, but suffers from a much larger background than the leptonic mode. We therefore only consider the fully leptonic decays of the  $W$  bosons in this work.

The two intermediate  $W$  bosons are required to be on-shell, namely their momenta satisfying  $q_i^2 = M_W^2$  with  $i = 1, 2$ . This condition is crucial for the separation of the different polarization contributions, because gauge invariance is guaranteed in this on-shell limit.

To make this on-shell phase space available, the invariant mass of the final-state leptons must be greater than  $2M_W$ . It is therefore important that this condition is also satisfied in the experimental analysis.

In simulation, the different polarizations of the  $W^+W^-$  pair can be separated using the double-pole approximation (DPA). This technique has been used for the  $ZZ$  [9],  $WZ$  [18, 10, 11], and  $W^+W^-$  [8, 12, 13, 17] processes up to NLO QCD+EW level. For the  $W^+W^-$  case, an NNLO QCD calculation has been performed [15].

The idea of the DPA can be understood by considering the unpolarized LO DPA amplitude:

$$\mathcal{A}_{\text{DPA}}^{\bar{q}q \rightarrow V_1 V_2 \rightarrow 4l} = \frac{1}{Q_1 Q_2} \sum_{\lambda_1, \lambda_2=1}^3 \mathcal{A}_{\text{LO}}^{\bar{q}q \rightarrow V_1 V_2}(\hat{k}_i, \lambda_1, \lambda_2) \mathcal{A}_{\text{LO}}^{V_1 \rightarrow l_1 l_2}(\hat{k}_i, \lambda_1) \mathcal{A}_{\text{LO}}^{V_2 \rightarrow l_3 l_4}(\hat{k}_i, \lambda_2), \quad (2)$$

with

$$Q_j = q_j^2 - M_{V_j}^2 + iM_{V_j}\Gamma_{V_j} \quad (j = 1, 2), \quad (3)$$

where  $M_{V_j}$  and  $\Gamma_{V_j}$  are the mass and the total decay width of the  $W$  bosons.

Compared to the full  $\bar{q}q \rightarrow 4l$  amplitudes, contributions from the non-doubly-resonant diagrams have been omitted. Another notable difference is the application of the on-shell phase space mapping

$$\text{on-shell mapping: } [k_i] \rightarrow [\hat{k}_i] \quad (4)$$

with  $i = \overline{1,6}$  for all external-state particles.  $k_i$  are the off-shell momenta. The mapped (or on-shell) momenta  $\hat{k}_i$  are all massless and satisfy the on-shell condition:

$$\hat{q}_1^2 = (\hat{k}_3 + \hat{k}_4)^2 = M_W^2, \quad \hat{q}_2^2 = (\hat{k}_5 + \hat{k}_6)^2 = M_W^2. \quad (5)$$

Solution for these on-shell momenta can be found if the off-shell momenta satisfy:

$$(k_3 + k_4 + k_5 + k_6)^2 \geq 4M_W^2, \quad (6)$$

as above mentioned.

The result of Eq. (2) is obtained from the key observation that the on-shell production amplitudes  $\mathcal{A}_{\bar{q}q \rightarrow V_1 V_2}$  and on-shell decay amplitudes  $\mathcal{A}_{V_i \rightarrow ll'}$  are individually gauge invariant. This is the reason for the application of the on-shell mapping. The DPA result of Eq. (2) can be thought of as an on-shell projection of an off-shell amplitude. This on-shell projection includes the following steps:

- Select only the  $V_1 V_2$  doubly-resonant Feynman diagrams.
- Replace the intermediate  $V_i$  propagators using:

$$V_i \text{ propagator: } P_i = \frac{-ig^{\mu\nu}}{Q_i} \rightarrow \frac{i}{Q_i} \sum_{\lambda=1}^3 \varepsilon_{\lambda}^{\mu*}(q_i) \varepsilon_{\lambda}^{\nu}(q_i), \quad (7)$$

$$g^{\mu\nu} = - \sum_{\lambda=1}^3 \varepsilon_{\lambda}^{\mu*}(k) \varepsilon_{\lambda}^{\nu}(k) + \frac{k^{\mu} k^{\nu}}{M_V^2}, \quad k = q_i, \quad (8)$$

where the 't Hooft-Feynman gauge has been used for simplicity. We can choose another gauge which can introduce a new term proportional to  $q_i^{\mu} q_i^{\nu}$  into  $P_i$ . This additional term cancels against the corresponding would-be Goldstone boson contribution. For the same reason, the last term proportional to  $k^{\mu} k^{\nu}$  in Eq. (8) can be safely removed. This cancellation is expected to occur at any order in a perturbation theory (see e.g. [14]).

- Perform the on-shell momenta mapping for the production amplitudes and decay amplitudes.

Eq. (2) provides a simple way to separate polarizations of the intermediate  $W$  bosons. We just need to select the desired  $(\lambda_1, \lambda_2)$  combination from the DPA amplitude. Specifically, we have

$$\begin{aligned} \mathcal{A}_{LL} &= \mathcal{A}_{\text{DPA}}(\lambda_1 = 2, \lambda_2 = 2), \\ \mathcal{A}_{LT} &= \mathcal{A}_{\text{DPA}}(\lambda_1 = 2, \lambda_2 = 1) + \mathcal{A}_{\text{DPA}}(\lambda_1 = 2, \lambda_2 = 3), \\ \mathcal{A}_{TL} &= \mathcal{A}_{\text{DPA}}(\lambda_1 = 1, \lambda_2 = 2) + \mathcal{A}_{\text{DPA}}(\lambda_1 = 3, \lambda_2 = 2), \\ \mathcal{A}_{TT} &= \mathcal{A}_{\text{DPA}}(\lambda_1 = 1, \lambda_2 = 1) + \mathcal{A}_{\text{DPA}}(\lambda_1 = 1, \lambda_2 = 3) \\ &\quad + \mathcal{A}_{\text{DPA}}(\lambda_1 = 3, \lambda_2 = 1) + \mathcal{A}_{\text{DPA}}(\lambda_1 = 3, \lambda_2 = 3). \end{aligned} \quad (9)$$

From this we see that the LT contribution is a coherent sum of the (2,1) and (2,3) polarized amplitudes. Similarly can be said for the TL and TT polarizations. The unpolarized amplitude reads:

$$\mathcal{A}_{\text{unpol}} = \mathcal{A}_{LL} + \mathcal{A}_{LT} + \mathcal{A}_{TL} + \mathcal{A}_{TT}, \quad (10)$$

which gives

$$\sigma_{\text{unpol}} = \sigma_{\text{LL}} + \sigma_{\text{LT}} + \sigma_{\text{TL}} + \sigma_{\text{TT}} + \sigma_{\text{pol-int}}, \quad (11)$$

where the last term is called the polarization interference. This interference is the interference between the LL, LT, TL, and TT modes. This interference vanishes for the integrated cross section in the case of fully inclusive decay products, namely the momenta of the decay products are not restricted [8]. If a particular distribution (e.g.  $p_{T,\ell}$ ) is considered, then the interference effect will show up at a given bin, even for a fully inclusive analysis. This is because the cross section of a specific bin is no longer inclusive.

The above on-shell projection has been extended up to NLO EW level in [9, 11, 12, 13, 17] for the inclusive diboson case and in [14] for the  $W^+W^+jj$  case. The case of QCD corrections is simpler as only radiative corrections to the initial-state particles are involved. NLO EW corrections are more complicated because radiative corrections occur for both initial and final state particles. Moreover, as the intermediate  $W$  bosons are on-shell soft divergences occur when a real or virtual photon is emitted from these  $W$  bosons. These divergences together with soft and collinear divergences from the initial and final state radiation have to be properly treated so that infrared-safe observables are obtained (see e.g. [19]). In this work, we have used the dipole subtraction method [19, 20] to deal with the infrared (i.e. soft or collinear) divergences. More details are provided in [11, 13, 17].

The polarized  $W^+W^-$  process was first calculated in [12, 13] at NLO EW using the four-flavor scheme, i.e. the bottom-quark induced processes were excluded. The main reason for this choice is to exclude the top-quark contribution which occurs starting from NLO in both QCD and EW corrections. At NLO, the processes of  $gb \rightarrow tW \rightarrow W^+W^-b$  (QCD) and  $\gamma b \rightarrow tW \rightarrow W^+W^-b$  (EW) occur. At NNLO,  $gg \rightarrow t\bar{t} \rightarrow W^+W^-bb$  and  $q\bar{q} \rightarrow t\bar{t} \rightarrow W^+W^-bb$  processes happen. They all produce polarized  $W^+W^-$  pairs. These contributions are large due to the top-quark resonances.

The definition of the inclusive  $W^+W^-$  production process is

$$pp \rightarrow W^+W^- + N \text{ jets} + M \text{ photons} + X, \quad (12)$$

with  $N \geq 0$ ,  $M \geq 0$ . A jet here can include all partons except the top quark. This definition includes the default  $q\bar{q}/gg \rightarrow W^+W^-$  mechanisms as well as the above top-quark induced ones. The  $t\bar{t}$  contribution is completely dominant due to its large cross section at the LHC.

In measurements, the top-quark contribution can be suppressed using jet cuts (e.g.  $p_{\text{jet-veto}}^T = 35 \text{ GeV}$ ) and then subtracted in the signal region using a partly data-driven method [21]. The remaining contribution is the default  $q\bar{q}/gg \rightarrow W^+W^-$  mechanisms, which are widely known in the community as the  $W^+W^-$  production signal.

For the SM prediction, the same procedure can be performed if the inclusive cross section of Eq. (12) is accurately known. The top-quark background contribution must be separately calculated and then subtracted from the inclusive result. In this way, the top-quark interference contribution is part of the signal and is consistent with the measurement. This definition of the  $W^+W^-$  signal in the five-flavor scheme (5FS) is discussed in detail in [22].

From a precision-calculation point of view, there is a good approach called the four-flavor scheme (4FS). In this scheme, the bottom quark is massive, and hence bottom jet is excluded in the inclusive cross section definition (see Eq. (12)). Bottom PDF is set to zero, hence no bottom quark in the initial state. This 4FS definition of the  $W^+W^-$  signal is free of the top-quark contribution by definition. The calculation is easier because the masses of the light quarks are set to zero, allowing for higher perturbative order computation. However, there is a mismatch between this definition and the measurement because there is still a bottom-induced contribution in the measurement result after the subtraction of the top-quark contribution.

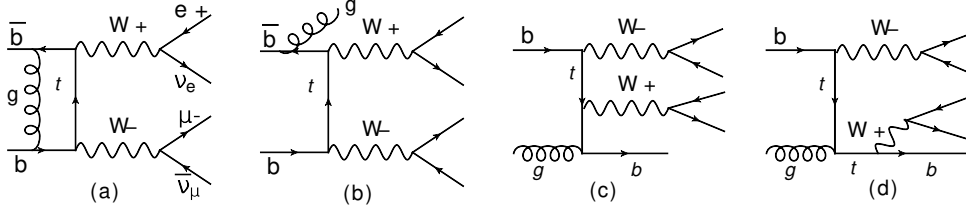


**Figure 2.** Various types of bottom-induced contributions to the inclusive  $W^+W^-$  production. (a,b,c) are of non- $tW$  origin, while (d) is of  $tW$  origin. The top-quark interference (or  $tW$  interference) is the interference between (c) and (d).

Moreover, the top-quark interference (i.e the signal-background interference) is part of the signal in the measurement result. This term is missing in the 4FS definition.

This point is illustrated in Fig. 2. The mismatch between the 4FS definition and the measurement includes contribution from diagrams (a,b,c) and the interference between (c) and (d).

We can account for this mismatch by calculating the bottom induced corrections separately. In this way we can make use of the precise calculation of the 4FS. This approach is well motivated because the bottom induced contribution is in most cases much smaller than the light-quark contribution. Moreover, as  $b$  jets can be tagged in experimental analyses, a separate treatment of the  $b$ -induced contribution is a good idea.

In this work, we include  $b$  jets in the definition of the inclusive  $W^+W^-$  production. Accordingly, the 5FS definition is used for the signal cross section. We will follow the same procedure as in the experimental measurement. Namely, the inclusive cross section including the top-quark contribution will firstly be calculated. Then, the on-shell top-quark contribution will be separately computed. The signal cross section is then obtained after the subtraction of the on-shell top-quark contribution. This subtraction has to be done for individual polarized cross sections. As our calculation is limited to NLO QCD+EW, the top-quark contribution includes only the  $tW$  mechanism. Details of this calculation are provided in [17].

### 3. Numerical results

In measurements, a jet veto (applying for all partons) is usually used to reduce the top-quark backgrounds, as done in the ATLAS case [21]. The problem with this choice is that using a jet veto increases the error of the theoretical prediction [23]. In the CMS measurement [24], a jet veto was used in the Sequential Cut but not in the Random Forest cut. Moreover, the number of  $b$ -tagged jets is required to be zero to reduce the top-quark backgrounds. In this way, jet veto is used only for the bottom induced contribution, thereby reducing the jet-veto error of the theoretical prediction as the  $b$ -induced cross section is small in most cases.

In the following, we will present the results for two cut setups: YesVeto and NoVeto. The YesVeto setup reads

$$p_{T,\ell} > 27 \text{ GeV}, \quad p_{T,\text{miss}} > 20 \text{ GeV}, \quad |\eta_\ell| < 2.5, \quad m_{e\mu} > 55 \text{ GeV}, \\ \text{jet veto (no jets with } p_{T,j} > 35 \text{ GeV and } |\eta_j| < 4.5), \quad (13)$$

while the NoVeto one is identical except that the jet-veto cut is removed. For the YesVeto case, the  $b$  jet is treated in the same way as the gluon or light-quark jets.

Results for the integrated cross sections are shown in Table 1 for the YesVeto and NoVeto cases. Unpolarized and polarized cross sections are provided for two cases: NoB, NoTW. Here NoB means the bottom-induced contribution is excluded. NoTW means the  $b$ -induced processes

	YesVeto				NoVeto			
	$\sigma_{\text{NoB}}$ [fb]	$\sigma_{\text{NoTW}}$ [fb]	$f_{\text{NoB}}$ [%]	$f_{\text{NoTW}}$ [%]	$\sigma_{\text{NoB}}$ [fb]	$\sigma_{\text{NoTW}}$ [fb]	$f_{\text{NoB}}$ [%]	$f_{\text{NoTW}}$ [%]
Unpol	218.47(3) $^{+2.2\%}_{-2.1\%}$	220.50(3) $^{+2.1\%}_{-2.0\%}$	100	100	327.94(4) $^{+5.4\%}_{-4.2\%}$	334.17(4) $^{+5.4\%}_{-4.1\%}$	100	100
$W_L^+ W_L^-$	14.34 $^{+1.8\%}_{-2.6\%}$	15.59 $^{+1.2\%}_{-2.2\%}$	6.6	7.1	18.68 $^{+4.1\%}_{-3.3\%}$	21.04(1) $^{+4.0\%}_{-2.9\%}$	5.7	6.3
$W_L^+ W_T^-$	24.79 $^{+1.9\%}_{-2.5\%}$	25.31 $^{+1.6\%}_{-2.5\%}$	11.3	11.5	43.33 $^{+6.0\%}_{-4.9\%}$	44.86(1) $^{+6.1\%}_{-4.8\%}$	13.2	13.4
$W_T^+ W_L^-$	25.47 $^{+2.1\%}_{-2.5\%}$	25.99 $^{+1.8\%}_{-2.4\%}$	11.7	11.8	44.22(1) $^{+6.2\%}_{-4.9\%}$	45.77(1) $^{+6.2\%}_{-4.8\%}$	13.5	13.7
$W_T^+ W_T^-$	152.59(3) $^{+2.2\%}_{-1.9\%}$	152.67(3) $^{+2.2\%}_{-1.9\%}$	69.8	69.2	221.43(3) $^{+5.3\%}_{-4.1\%}$	222.80(3) $^{+5.3\%}_{-4.1\%}$	67.5	66.7
Pol-int	1.27(4)	0.93(4)	0.6	0.4	0.28(5)	-0.30(5)	0.1	-0.1

**Table 1.** Results for the unpolarized and polarized DPA cross sections using the YesVeto and NoVeto cut setups. These results are taken from [17].

are included and the on-shell  $tW$  contribution is subtracted. This is the signal cross section as measured in ATLAS and CMS. The polarization fractions defined as  $f_i = \sigma_i/\sigma_{\text{unpol}}$  for the polarization  $i$  are also provided. The polarization interference is provided in the last row. The scale uncertainties are shown in percent as upper and lower indices on the value of the cross section. These uncertainties are calculated using the direct variation method of the factorization and renormalization scales (seven-point method, see [17] for details). The Monte-Carlo errors are provided in the round parentheses if significant. We see that the  $b$ -induced contribution increases the LL fraction by 7.6% and 10.5% for the YesVeto and NoVeto cases, respectively.

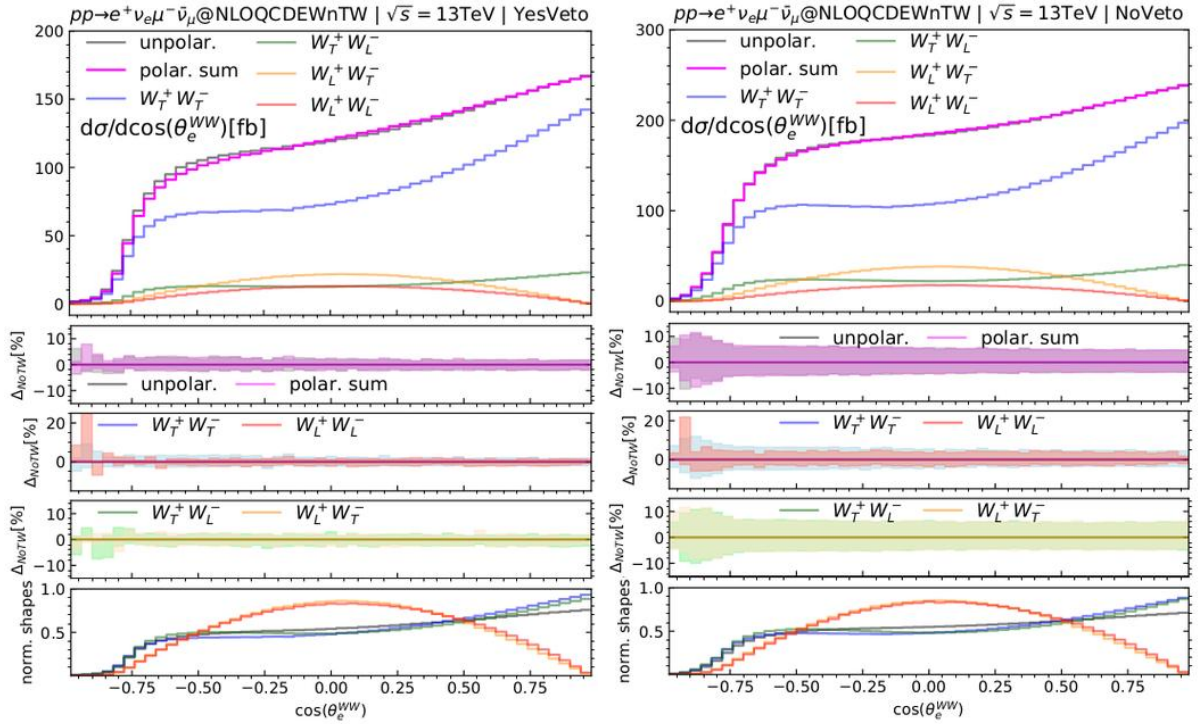


**Figure 3.** Differential polarized cross sections in  $\cos \theta_e^{WW}$  (see text) for YesVeto and NoVeto cut setups. Results are taken from [17].

Example results of differential cross sections are shown in Fig. 3. The kinematic variable here is  $\cos\theta_e^{WW}$ , the electron polar angle calculated in the  $WW$  center-of-mass frame. This is however not a normal polar angle.  $\theta_e^{WW}$  is the angle between the spatial momentum  $\vec{p}_e^{W\text{-rest}}$  determined in the  $W^+$ -rest frame and the spatial momentum  $\vec{p}_{W^+}^{WW}$  determined in the  $WW$  center-of-mass frame. As the Lorentz boost order is important, we have to boost the relevant momenta to the  $WW$  frame first, and then from here boost to the  $W^+$  rest frame. If we do not follow this order and jump directly to the  $W^+$  rest frame from e.g. the LAB frame, then the obtained  $\vec{p}_e^{W\text{-rest}}$  would be wrong.

This polar angle is of particular important in the polarization measurement. This is because it is sensitive to the polarization of the parent gauge boson, i.e. the  $W^+$  in this discussion. It is not sensitive to the polarization of the other gauge boson. This is why we get almost identical normalized shapes for the  $W_L^+W_L^-$  and  $W_L^+W_T^-$  cases, as can be seen from the bottom panels in Fig. 3. Similarly, the shapes of the  $W_T^+W_L^-$  and  $W_T^+W_T^-$  cases are also almost identical. The distinct difference in shape between the  $W_L^+W_L^-$  and  $W_T^+W_L^-$  cases shows the power of this polar angle. Likewise, to distinguish the polarizations of the  $W^-$  boson, the muon polar angle  $\cos\theta_\mu^{WW}$  should be used.

The three small panels below the big panel show the relative scale uncertainties of the cross sections provided in the big panel. The uncertainties are much smaller for the YesVeto case. This is due to an accidental cancellation of different NLO corrections at the chosen value of the jet-veto threshold (35 GeV), see [23]. It turns out that the cancellation is largest around this value, leading to small values of the scale uncertainties. As discussed in [17], the scale uncertainties provided here for the YesVeto case are likely to be underestimated. Care must therefore be taken when using these values.

## 4. Conclusions

In this report, we have discussed a calculation method for the inclusive polarized  $W^+W^-$  production signal at the LHC in the five-flavor scheme. The method is applicable at NLO QCD+EW level. The key idea is to calculate the on-shell top-quark contribution separately and subtract it from the inclusive cross section. Example results have been presented for the integrated cross sections and a differential cross section for two cut setups, with and without a jet veto.

## Acknowledgments

The authors would like to thank the workshop organizers for organizing this nice event. This work is funded by Phenikaa University under grant number PU2023-1-A-18.

## References

- [1] ATLAS collaboration, G. Aad et al., *Observation of gauge boson joint-polarisation states in  $W^\pm Z$  production from  $pp$  collisions at  $\sqrt{s} = 13$  TeV with the ATLAS detector*, *Phys. Lett. B* **843** (2023) 137895 [2211.09435].
- [2] ATLAS collaboration, G. Aad et al., *Studies of the energy dependence of diboson polarization fractions and the Radiation Amplitude Zero effect in  $WZ$  production with the ATLAS detector*, *2402.16365*.
- [3] ATLAS collaboration, G. Aad et al., *Evidence of pair production of longitudinally polarised vector bosons and study of CP properties in  $ZZ \rightarrow 4\ell$  events with the ATLAS detector at  $\sqrt{s} = 13$  TeV*, *JHEP* **12** (2023) 107 [2310.04350].
- [4] CMS collaboration, A. M. Sirunyan et al., *Measurements of production cross sections of polarized same-sign  $W$  boson pairs in association with two jets in proton-proton collisions at  $\sqrt{s} = 13$  TeV*, *Phys. Lett. B* **812** (2021) 136018 [2009.09429].
- [5] M. Hoppe, M. Schönherr and F. Siegert, *Polarised cross sections for vector boson production with SHERPA*, *2310.14803*.
- [6] G. Pelliccioli and G. Zanderighi, *Polarised-boson pairs at the LHC with NLOPS accuracy*, *Eur. Phys. J. C* **84** (2024) 16 [2311.05220].



- [7] M. Javurkova, R. Ruiz, R. C. L. de Sá and J. Sandesara, *Polarized ZZ pairs in gluon fusion and vector boson fusion at the LHC*, *Phys. Lett. B* **855** (2024) 138787 [2401.17365].
- [8] A. Denner and G. Pelliccioli, *Polarized electroweak bosons in  $W^+W^-$  production at the LHC including NLO QCD effects*, *JHEP* **09** (2020) 164 [2006.14867].
- [9] A. Denner and G. Pelliccioli, *NLO EW and QCD corrections to polarized ZZ production in the four-charged-lepton channel at the LHC*, *JHEP* **10** (2021) 097 [2107.06579].
- [10] D. N. Le and J. Baglio, *Doubly-polarized WZ hadronic cross sections at NLO QCD + EW accuracy*, *Eur. Phys. J. C* **82** (2022) 917 [2203.01470].
- [11] D. N. Le, J. Baglio and T. N. Dao, *Doubly-polarized WZ hadronic production at NLO QCD+EW: calculation method and further results*, *Eur. Phys. J. C* **82** (2022) 1103 [2208.09232].
- [12] A. Denner, C. Haitz and G. Pelliccioli, *NLO EW corrections to polarised  $W^+W^-$  production and decay at the LHC*, *Phys. Lett. B* **850** (2024) 138539 [2311.16031].
- [13] T. N. Dao and D. N. Le, *NLO electroweak corrections to doubly-polarized  $W^+W^-$  production at the LHC*, *Eur. Phys. J. C* **84** (2024) 244 [2311.17027].
- [14] A. Denner, C. Haitz and G. Pelliccioli, *NLO EW and QCD corrections to polarised same-sign WW scattering at the LHC*, *JHEP* **11** (2024) 115 [2409.03620].
- [15] R. Poncelet and A. Popescu, *NNLO QCD study of polarised  $W^+W^-$  production at the LHC*, *JHEP* **07** (2021) 023 [2102.13583].
- [16] A. Denner, C. Haitz and G. Pelliccioli, *NLO QCD corrections to polarized diboson production in semileptonic final states*, *Phys. Rev. D* **107** (2023) 053004 [2211.09040].
- [17] T. N. Dao and D. N. Le, *Polarized  $W^+W^-$  pairs at the LHC: Effects from bottom-quark induced processes at NLO QCD + EW*, *Eur. Phys. J. C* **85** (2025) 108 [2409.06396].
- [18] A. Denner and G. Pelliccioli, *NLO QCD predictions for doubly-polarized WZ production at the LHC*, *Phys. Lett. B* **814** (2021) 136107 [2010.07149].
- [19] S. Catani and M. Seymour, *A General algorithm for calculating jet cross-sections in NLO QCD*, *Nucl. Phys.* **B485** (1997) 291 [hep-ph/9605323].
- [20] S. Dittmaier, *A General approach to photon radiation off fermions*, *Nucl. Phys.* **B565** (2000) 69 [hep-ph/9904440].
- [21] ATLAS collaboration, M. Aaboud et al., *Measurement of fiducial and differential  $W^+W^-$  production cross-sections at  $\sqrt{s} = 13$  TeV with the ATLAS detector*, *Eur. Phys. J. C* **79** (2019) 884 [1905.04242].
- [22] T. Gehrmann, M. Grazzini, S. Kallweit, P. Maierhöfer, A. von Manteuffel, S. Pozzorini et al.,  *$W^+W^-$  Production at Hadron Colliders in Next to Next to Leading Order QCD*, *Phys. Rev. Lett.* **113** (2014) 212001 [1408.5243].
- [23] I. W. Stewart and F. J. Tackmann, *Theory Uncertainties for Higgs and Other Searches Using Jet Bins*, *Phys. Rev. D* **85** (2012) 034011 [1107.2117].
- [24] CMS collaboration, A. M. Sirunyan et al.,  *$W^+W^-$  boson pair production in proton-proton collisions at  $\sqrt{s} = 13$  TeV*, *Phys. Rev. D* **102** (2020) 092001 [2009.00119].